Dark matter distribution in the Coma cluster from galaxy kinematics: breaking the mass-anisotropy degeneracy

Ewa L. Lokas, Gary A. Mamon

Mon. Not. R. Astron. Soc. **343,** 401–412 (2003)

Dark matter distribution in the Coma cluster from galaxy kinematics: breaking the mass–anisotropy degeneracy

Ewa L. Łokas[1]★ and Gary A. Mamon[2,3]★

[1]*Copernicus Astronomical Center, Bartycka 18, 00–716 Warsaw, Poland*
[2]*Institut d'Astrophysique de Paris (CNRS UMR 7095), 98 bis Bd Arago, F-75014 Paris, France*
[3]*GEPI (CNRS UMR 8111), Observatoire de Paris, F-92195 Meudon, France*

Accepted 2003 April 1. Received 2003 April 1; in original form 2003 February 21

ABSTRACT

We study velocity moments of elliptical galaxies in the Coma cluster using Jeans equations. The dark matter distribution in the cluster is modelled by a generalized formula based upon the results of cosmological N-body simulations. Its inner slope (cuspy or flat), concentration and mass within the virial radius are kept as free parameters, as well as the velocity anisotropy, assumed independent of position. We show that the study of line-of-sight velocity dispersion alone does not allow us to constrain the parameters. By a joint analysis of the observed profiles of velocity dispersion and kurtosis, we are able to break the degeneracy between the mass distribution and velocity anisotropy. We determine the dark matter distribution at radial distances larger than 3 per cent of the virial radius and we find that the galaxy orbits are close to isotropic. Due to limited resolution, different inner slopes are found to be consistent with the data and we observe a strong degeneracy between the inner slope α and concentration c; the best-fitting profiles have the two parameters related with $c = 19-9.6\alpha$. Our best-fitting Navarro–Frenk–White profile has concentration $c = 9$, which is 50 per cent higher than standard values found in cosmological simulations for objects of similar mass. The total mass within the virial radius of $2.9h_{70}^{-1}$ Mpc is $1.4 \times 10^{15} h_{70}^{-1}$ $M_\odot$ (with 30 per cent accuracy), 85 per cent of which is dark. At this distance from the cluster centre, the mass-to-light ratio in the blue band is $351h_{70}$ solar units. The total mass within the virial radius leads to estimates of the density parameter of the Universe, assuming that clusters trace the mass-to-light ratio and baryonic fraction of the Universe, with $\Omega_0 = 0.29 \pm 0.1$.

Key words: methods: analytical – galaxies: clusters: individual: Coma – galaxies: kinematics and dynamics – dark matter.

1 INTRODUCTION

The Coma cluster of galaxies (Abell 1656) is one of the most extensively studied in our neighbourhood (see, for example, Biviano 1998, and references therein). Starting with the seminal paper of Kent & Gunn (1982) significant effort went into dynamical modelling of the cluster. In the early studies based on about 300 galaxy velocities, only velocity dispersion was modelled and it was most often assumed that the mass follows light and that the galaxies are on isotropic orbits. Merritt (1987) has shown that, if a larger variety of models is allowed, there is a strong degeneracy between the dark matter distribution and velocity anisotropy and many models can be shown to be consistent with the data. Without any prior knowledge of the mass distribution, even considering higher velocity moments would probably not be of much help.

Recently, due to theoretical progress mainly by the means of N-body simulations, our knowledge on possible dark matter distributions within gravitationally bound objects has improved significantly. There seems to be general agreement at least as to the behaviour of dark matter density profiles at large radial distances ($\varrho \propto r^{-3}$). Whether the inner dark matter density profile is $\varrho \propto r^{-1}$ (as in the so-called universal profile advocated by Navarro, Frenk & White 1997) or $\varrho \propto r^{-3/2}$ (as preferred by Moore et al. 1998; see also Fukushige & Makino 1997) or is flat (as suggested by the observed rotation curves of dwarf and low surface brightness galaxies, e.g. McGaugh & de Blok 1998) is still a matter of debate; a recent analysis by Jimenez, Verde & Oh (2003) of high-resolution rotation curves of spiral galaxies shows that 2/3 of the sample can be accounted by Navarro–Frenk–White (NFW) profiles, but 2/3 also with a flat core. We therefore consider a generalized profile with different inner slopes and also allow for different dark matter concentrations. We constrain this variety of dark matter density profiles by modelling velocity moments of galaxies. In addition to constraints from the

★E-mail: lokas@camk.edu.pl (ELL); gam@iap.fr (GAM)

line-of-sight velocity dispersion profile, we incorporate constraints from the fourth velocity moment, the kurtosis.

The NFW profile has been found to be consistent with the total mass distribution inferred from the galaxy data combined from many clusters in the Canadian Network for Observational Cosmology 1 (CNOC1; van der Marel et al. 2000) and ESO Nearby Abell Cluster Survey (ENACS; Biviano et al. 2003). Although van der Marel et al. (2000) considered higher velocity moments, they did not apply them rigorously to further constrain the mass distribution. Studies based upon X-rays, assuming that the hot X-ray emitting gas is in hydrostatic equilibrium in a spherical potential, usually lead to NFW-like cuspy centres (McLaughlin 1999; Tamura et al. 2000; Sato et al. 2000). The studies based on gravitational lensing focus on the inner shape of the density profile. The slopes agree with the NFW prediction in some studies (e.g. Broadhurst et al. 2000) while one team finds a preference for a flat core (Tyson, Kochanski & dell'Antonio 1998; see also Williams, Navarro & Bartelmann 1999). Note that the Coma cluster is too close for its mass profile to be probed through gravitational lensing.

The amount of galaxy velocity as well as brightness and morphological type measurements for the members of Coma has increased over the last two decades, making it possible to analyse separately the samples of elliptical and spiral galaxies. While ellipticals appear to be in dynamical equilibrium justifying the application of Jeans formalism to study their velocity moments, most of the spirals are probably infalling on to the cluster. The modelling of the infall of spirals will be presented in the follow-up study.

The paper is organized as follows. In Section 2 we describe our data. In Section 3 we present our assumptions concerning the matter content of the cluster, i.e. the distributions of galaxies, gas and dark matter. In Section 4 we outline our formalism for modelling the velocity moments of elliptical galaxies based on Jeans equations. In Section 5 we present its application to constrain the parameters of our model, in particular the distribution of dark matter in the cluster. A discussion follows in Section 6.

2 THE DATA

We have searched the NASA/IPAC Extragalactic Data Base (NED) for galaxies within 300 arcmin of RA $= 12^{\rm h}59^{\rm m}35\overset{\rm s}{.}7$, Dec. $= +27^\circ57'33''$ (J2000), i.e. the position of the elliptical galaxy NGC 4874, well established as the centre of the Coma cluster (Kent & Gunn 1982). The galaxies were required to have velocities between 3000 and 11 000 km s^{-1} (given the velocity dispersions we will find below, this velocity range extends to $\gtrsim 4\sigma$). For the calculation of the velocity moments and the subsequent study of kinematics, we remove from the list galaxy pairs and known members of pairs (as given by the NED), as we wish to probe the global cluster potential but not its local enhancements. We then obtain a sample of 1068 galaxies shown in the upper panel of Fig. 1 as points in the plane of velocity versus distance from the centre of the cluster. To determine the membership of galaxies in the cluster we proceed in a similar fashion as Kent & Gunn (1982). As can be seen from Fig. 1, the members of the cluster are well separated from the foreground and background galaxies in velocity space. We have therefore selected the probable members of Coma as lying within the two curves shown in Fig. 1, symmetric with respect to $v = 7000$ km s^{-1}, the value close to the mean velocity of the cluster. This procedure leaves us with 967 galaxies. For the determination of the luminosity distribution, we keep the members of galaxy pairs and remove a few galaxies for which no magnitude estimate is available (they may contribute to the calculation of velocity moments however). We then proceed with the membership determination as before.

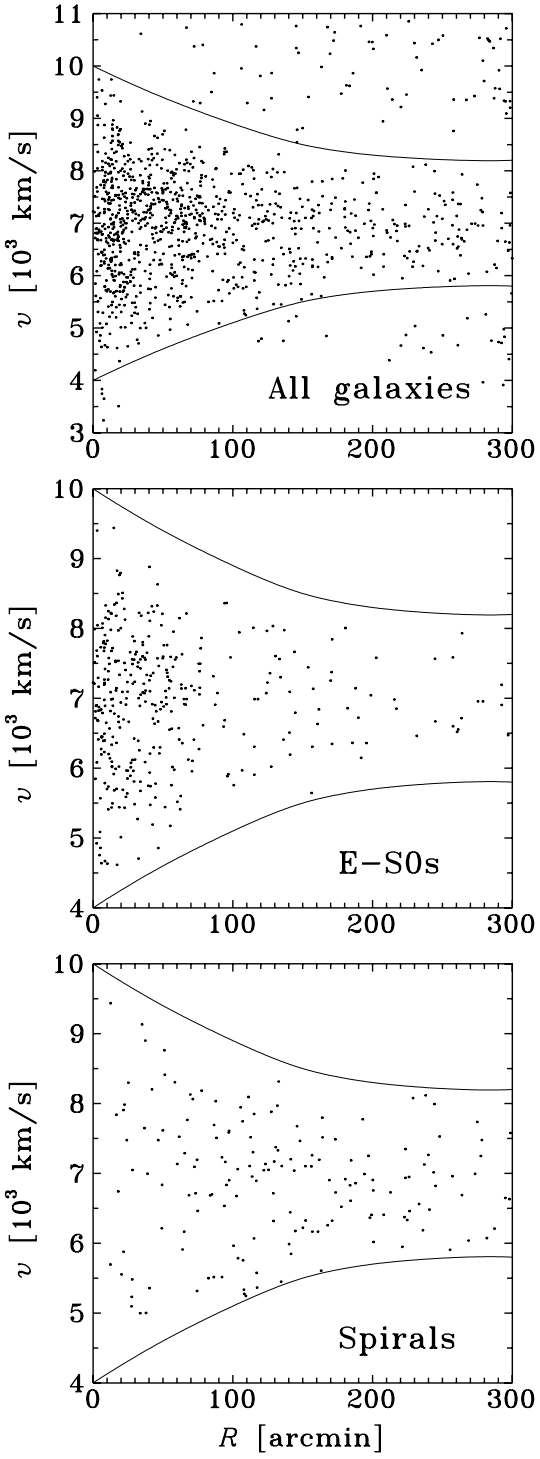

Figure 1. Upper panel: 1068 galaxies selected from the NED data base within 300 arcmin from NGC 4874 with heliocentric velocities between 3000 and 11 000 km s^{-1}. Middle panel: 355 E-S0 galaxies, members of Coma. Lower panel: 163 spiral galaxies, members of Coma. The curves indicate envelopes of the cluster.

It is generally believed that only early-type (E-S0) galaxies can be considered in dynamical equilibrium within a cluster in opposition to spirals which are believed to be infalling (e.g. Tully & Shaya

1984; Huchra 1985). We therefore construct separate samples of E-S0 and spiral galaxies. The morphological type of the galaxies has been determined by consulting the NED, SIMBAD and LEDA data bases. Among the 967 galaxies belonging to Coma and selected for the analysis of the velocity moments, we find 355 E-S0s, 163 spirals and 449 other galaxies for which the morphological classification is unknown or uncertain. As already noticed by Kent & Gunn (1982), the cluster shows a clear morphological segregation. The distributions of E-S0s and spirals in the R–v plane are shown in the middle and lower panel of Fig. 1. Comparison of the two plots reveals that while E-S0s cluster and dominate in the central parts of Coma and are not numerous at radial distances larger than 80 arcmin, spirals are more uniformly distributed and underrepresented in the central region. Similar subsamples are constructed for the analysis of the luminosity distribution. Note that iterating on the mean velocity and establishing new symmetric envelopes for the cluster in the observed phase space has virtually no effect on the cluster membership. We note a possible group of galaxies at $R < 10$ arcmin and $v < 4000$ km s^{-1} that might have been missed, but contributes little to the central internal kinematics.

3 THE MATTER CONTENT OF THE CLUSTER

3.1 The mass in stars

The mass contributed by the stars in galaxies is estimated as follows. Ideally, we would like to determine the surface luminosity distribution separately for different morphological types of galaxies, as transforming luminosity into mass requires mass-to-light ratios, which are known to vary with morphological type. However, as we do not know the morphological type for roughly half the galaxies in our sample, we would have to assume for these galaxies some mean value of the mass-to-light ratio. Combining then the fits for the three classes of galaxies, E-S0s, spirals and those of unknown type, would produce large uncertainties, as the luminosity distribution for spirals turns out to be quite noisy. Therefore, in determining the total stellar mass distribution, we fit the luminosity distribution for all galaxies and then translate it to the mass distribution using a mean mass-to-light ratio.

Magnitudes are transformed into luminosities assuming that all galaxies are at the same distance associated with the mean velocity of the Coma cluster. Adopting a heliocentric velocity of Coma of 6925 km s^{-1} (Struble & Rood 1999), and correcting for the velocity of the Sun with respect to the Local Group and for the Local Group infall on to Virgo, we obtain for Coma a Hubble flow velocity of 7093 km s^{-1}, which, for a Hubble constant of $H_0 = 70$ km s^{-1} Mpc^{-1} (assumed throughout this paper) gives a distance of 101.3 Mpc and a distance modulus of 35.03 (neglecting the peculiar velocity of the Coma cluster).

As mentioned in the previous section, our sample of galaxies for the luminosity analysis is different from that used for the calculation of velocity moments, as we no longer exclude the members of pairs. Now, we have 985 galaxies that belong to Coma, among which are 366 E-S0s and 167 spirals. The surface luminosity profile of all galaxies is then determined by placing 60 galaxies per radial bin. The resulting distribution is shown as filled symbols in Fig. 2. The open symbols in the figure show a similar result for just E-S0 galaxies but this time with 30 galaxies per radial bin. This second distribution will be needed in the modelling of the velocity moments as the distribution of our tracer population.

The data shown in Fig. 2 do not indicate any presence of a core in the surface luminosity distributions, hence we fit them with projections of cuspy profiles. For both samples, of all galaxies as well as early-type ones, the distributions have a changing slope, so we fit them with a projection of the NFW profile (Bartelmann 1996; see also Section 2.5 of Łokas & Mamon 2001). The fit is done by χ^2 minimization taking all points with equal weights (although we do not know the errors of the magnitude measurements, we expect them to be similar for galaxies in each bin). The three-dimensional (3D) luminosity density will then be

$$l(r) = \frac{l_\star}{(r/r_S)(1 + r/r_S)^2} \tag{1}$$

where the normalization constant $l_\star$ and the scale radius r_S are the two fitting parameters. For the sample of all galaxies we obtain $l_\star = 9.05 \times 10^7$ L$_\odot$ arcmin^{-3} and $r_S = 14.4$ arcmin. For the E-S0s we have $l_\star = 3.55 \times 10^8$ L$_\odot$ arcmin^{-3} and $r_S = 7.05$ arcmin so this distribution turns out to be more concentrated and therefore steeper. It might be interesting to note that the *number* density distribution of the galaxies in our sample is less steep in the centre than the *luminosity* density distribution and can be approximated by a profile with a core. The steeper distribution of luminosity is probably mainly due to the presence of bright ellipticals in the centre of the cluster (see Fig. 1).

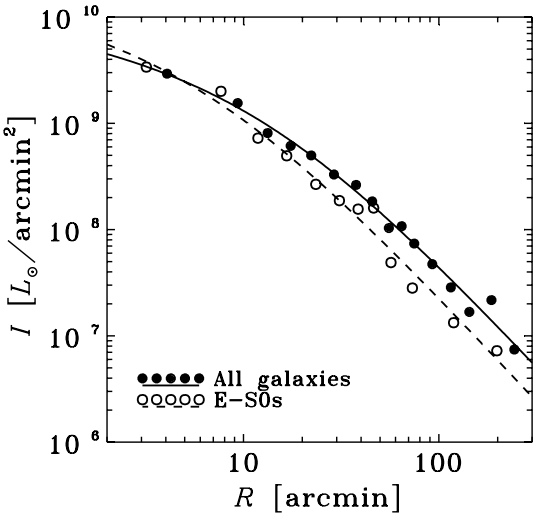

Figure 2. The surface luminosity distribution data together with the best-fitting projected NFW profiles for all 985 galaxies (filled symbols and solid line) and the 366 known E-S0s among them (open symbols and dashed line).

Integrating the luminosity distribution (1) and multiplying by the appropriate mass-to-light ratio in the blue band, Υ, we obtain the mass distribution associated with the stars in galaxies

$$M_G(r) = 4\pi l_\star \Upsilon r_S^3 \left(\ln \frac{r + r_S}{r_S} - \frac{r}{r + r_S} \right). \tag{2}$$

We adopt the mass-to-light ratio in blue band for E-S0s of $\Upsilon_E = 8$ M$_\odot$/L$_\odot$ and for spirals $\Upsilon_S = 3$ M$_\odot$/L$_\odot$. For the mass distribution of all galaxies we take the weighted mean of Υ. Because, for galaxies with known morphological type, the E-S0s and spirals appear in the proportions of 2.2:1, then assuming that the same proportion holds for the whole population, the mean mass-to-light ratio amounts to $\Upsilon_G = (2.2\Upsilon_E + \Upsilon_S)/3.2 = 6.43$ M$_\odot$/L$_\odot$.

3.2 The gas distribution

To approximate the contribution of the gas to the mass in the cluster we make use of the X-ray surface brightness distribution which can be well approximated by the following formula

$$S(r) = S_0 \left[1 + \left(\frac{r}{r_c}\right)^2\right]^{-3b+1/2}. \quad (3)$$

Briel, Henry & Böhringer (1992) analysed the *ROSAT* observations of Coma out to 100 arcmin in the energy band of 0.5–2.4 keV and obtained the following best-fitting parameters: $S_0 = 4.6 \times 10^{-13}$ erg cm^{-2} s^{-1} arcmin^{-2}, $b = 0.75$ and the core radius $r_c = 10.5$ arcmin. Assuming that the radiation is produced by bremsstrahlung, this distribution is obtained by projecting the 3D emissivity integrated over the energy band and assuming that the gas is approximately isothermal. As the emissivity is proportional to the square of the number density of electrons in the gas n, we obtain

$$n(r) = n_0 \left[1 + \left(\frac{r}{r_c}\right)^2\right]^{-3b/2}, \quad (4)$$

where the central electron density (with $h = 0.7$) is $n_0 = 3.42 \times 10^{-3}$ cm^{-3} (Briel et al. 1992; Henry & Henriksen 1986). Integrating equation (4) and multiplying by the mass per electron we obtain the mass distribution associated with the gas

$$M_g(r) = \frac{4}{3}\pi n_0 (m_e + \gamma m_p) r^3 \, {}_2F_1\left(\frac{3}{2}, \frac{3b}{2}; \frac{5}{2}; -\frac{r^2}{r_c^2}\right), \quad (5)$$

where ${}_2F_1$ is the hypergeometric function and γm_p with $\gamma = 1.136$ is the mean mass of the positively charged ion in the gas per unit charge (m_p being the proton mass), assuming the gas has the primordial composition with helium abundance of $Y_{He} = 0.23$–0.24.

Equation (3) for the surface brightness is the same as that appearing in the so-called β-model (we have replaced β by b to avoid confusion with the anisotropy parameter of the next section); however, we do not accept all the assumptions of the model here concerning, for example, the relation between the gas and galaxy distributions. The only assumption going into the derivation of the gas mass distribution in equation (5), besides spherical symmetry, is that the gas is isothermal, which is justified by recent observations of Coma with *XMM-Newton* by Arnaud et al. (2001), who find very little temperature variation, at least in the central region of radius 20 arcmin.

3.3 Dark matter

We study different possible density distributions of dark matter described by the following general formula

$$\rho(r) = \frac{\rho_{char}}{(r/r_s)^\alpha (1 + r/r_s)^{3-\alpha}}, \quad (6)$$

where ρ_{char} is a constant characteristic density, and r_s is the scale radius of the dark matter (in general different from that of the luminous distribution, r_S). The profiles differ by the inner slope $r^{-\alpha}$ but have a common outer limiting behaviour of r^{-3}. We will consider α values limited by $0 \leqslant \alpha \leqslant 3/2$, which covers a wide range of possible inner profiles: from very steep to core-like. The cuspy profiles of $\alpha > 0$ are motivated by the results of cosmological N-body simulations. The profile with $\alpha = 1$ corresponds to the so-called universal profile proposed by NFW as a fit to the profiles of simulated haloes, while the profile with $\alpha = 3/2$ is identical to that following from higher-resolution simulations of Moore et al. (1998). The core profile with $\alpha = 0$ is favoured by some observations of galaxies and clusters and is very similar (but not identical) to the profile proposed by Burkert (1995).

The scale radius r_s introduced in equation (6) marks the distance from the centre of the object where the profile has a slope equal to the average of the inner and outer slope: $r^{-(3+\alpha)/2}$. The other parameter that controls the shape of the profile is the concentration

$$c = \frac{r_v}{r_s}, \quad (7)$$

where r_v is the virial radius, i.e. the distance from the centre of the halo within which the mean density is Δ_c times the present critical density, $\rho_{crit,0}$. Although in most cosmological N-body simulations $\Delta_c = 200$ is assumed and kept constant, the value, following from the spherical collapse model, depends on the underlying cosmology, e.g. $\Delta_c \approx 178$ is valid for the Einstein–de Sitter model, while, for the currently most popular Λ cold dark matter (CDM) model with $\Omega_M = 0.3$ and $\Omega_\Lambda = 0.7$, we have $\Delta_c \approx 102$ (Eke, Cole & Frenk 1996; Łokas & Hoffman 2001). We will keep $\Delta_c = 102$ in the following.

The concentration of simulated dark matter haloes has been observed to depend on the virial mass. Jing & Suto (2000) tested the relation $c(M_v)$ for the masses of the order of normal galaxies and clusters in the case of density profiles with $\alpha = 1$ and $\alpha = 3/2$ and found concentrations slowly decreasing with mass (thus confirming the original observation of NFW) and lower for $\alpha = 3/2$ than for $\alpha = 1$. The only study using the value of Δ_c appropriate for a given cosmological model is that of Bullock et al. (2001) who found the profiles of presently forming haloes to be well fitted by the NFW formula with concentrations depending on mass in the ΛCDM model with the above parameters approximately as

$$c(M_v) = 5.95 \left(\frac{M_v}{10^{15} h^{-1}\,M_\odot}\right)^{-0.122}. \quad (8)$$

In the following, we will treat the concentration as a free parameter using this relation to guide us as to the order of magnitude of c.

We normalize the density profile (6) so that the mass within r_v is equal to the so-called virial mass

$$M_v = \frac{4}{3}\pi r_v^3 \Delta_c \rho_{crit,0}. \quad (9)$$

The characteristic density of equation (6) then becomes

$$\rho_{char} = \frac{(3-\alpha)\Delta_c \rho_{crit,0} c^\alpha}{3 F_\alpha(c)}, \quad (10)$$

where $F_\alpha(c)$ is given by the hypergeometric function

$$F_\alpha(x) = {}_2F_1(3-\alpha, 3-\alpha; 4-\alpha; -x) = \begin{cases} \frac{3}{x^3}\left[\ln(1+x) - \frac{x}{2}\frac{(2+3x)}{(1+x)^2}\right] & (\alpha = 0) \\ \frac{5}{x^{5/2}}\left[\sinh^{-1}\sqrt{x} - \frac{\sqrt{x}}{3}\frac{3+4x}{(1+x)^{3/2}}\right] & (\alpha = 1/2) \\ \frac{2}{x^2}\left[\ln(1+x) - \frac{x}{1+x}\right] & (\alpha = 1) \\ \frac{3}{x^{3/2}}\left[\sinh^{-1}\sqrt{x} - \sqrt{\frac{x}{1+x}}\right] & (\alpha = 3/2). \end{cases} \quad (11)$$

The dark mass distribution following from equations (6), (9) and (10) is

$$M_D(s) = M_v s^{3-\alpha} \frac{F_\alpha(cs)}{F_\alpha(c)}, \quad (12)$$

where we introduced $s = r/r_v$.

4 MODELLING OF THE VELOCITY MOMENTS

The purpose of this work is to constrain the distribution of dark matter in the Coma cluster by studying the velocity moments of the

population of elliptical galaxies in the cluster which we believe to be in equilibrium (thus neglecting radial streaming motions). We defer to a later paper the kinematical study of spiral galaxies in the context of infall. We will also assume that the system is spherically symmetric and that there are no net streaming motions (e.g. no rotation) so that the odd velocity moments vanish.

At second order, the two distinct moments are $\overline{v_r^2}$ and $\overline{v_\theta^2} = \overline{v_\phi^2}$, which we will denote hereafter by σ_r^2 and σ_θ^2, respectively. They can be calculated from the lowest-order Jeans equation (e.g. Binney & Mamon 1982)

$$\frac{\mathrm{d}}{\mathrm{d}r}\left(\nu\sigma_r^2\right) + \frac{2\beta}{r}\nu\sigma_r^2 = -\nu\frac{\mathrm{d}\Phi}{\mathrm{d}r}, \tag{13}$$

where ν is the 3D density distribution of the tracer population and Φ is the gravitational potential. We will solve equation (13) assuming the anisotropy parameter

$$\beta = 1 - \frac{\sigma_\theta^2(r)}{\sigma_r^2(r)} \tag{14}$$

to be constant with $-\infty < \beta \leqslant 1$. This model covers all interesting possibilities from radial orbits ($\beta = 1$) to isotropy ($\beta = 0$) and circular orbits ($\beta \to -\infty$).

The solution of the lowest-order Jeans equation with the boundary condition $\sigma_r \to 0$ at $r \to \infty$ for $\beta = \text{const}$ is

$$\nu\sigma_r^2(\beta = \text{const}) = r^{-2\beta}\int_r^\infty r^{2\beta}\nu\frac{\mathrm{d}\Phi}{\mathrm{d}r}\mathrm{d}r. \tag{15}$$

However, the measurable quantity is the line-of-sight velocity dispersion obtained from the 3D velocity dispersion by integrating along the line of sight (Binney & Mamon 1982)

$$\sigma_{\rm los}^2(R) = \frac{2}{I(R)}\int_R^\infty\left(1-\beta\frac{R^2}{r^2}\right)\frac{\nu\sigma_r^2 r}{\sqrt{r^2-R^2}}\mathrm{d}r, \tag{16}$$

where $I(R)$ is the surface distribution of the tracer and R is the projected radius. Introducing equation (15) into equation (16) and inverting the order of integration, we obtain

$$\sigma_{\rm los}^2(R) = \frac{2G}{I(R)}\int_R^\infty \mathrm{d}x\,\nu(x)M(x)x^{2\beta-2} \times\int_R^x \mathrm{d}y\left(1-\beta\frac{R^2}{y^2}\right)\frac{y^{-2\beta+1}}{\sqrt{y^2-R^2}}, \tag{17}$$

where $M(x)$ is the mass distribution and we used new variables x and y instead of r to avoid confusion. The calculation of $\sigma_{\rm los}$ can then be reduced to one-dimensional numerical integration of a formula involving special functions for arbitrary $\beta = \text{const}$.

It has been established that by studying $\sigma_{\rm los}(R)$ alone we cannot uniquely determine the properties of a stellar system. In fact, systems with different densities and velocity anisotropies can produce identical $\sigma_{\rm los}(R)$ profiles (see, for example, Merrifield & Kent 1990; Merritt 1987). It is therefore interesting to consider higher-order moments of the velocity distribution. For the fourth-order moments, the three distinct components $\overline{v_r^4}$, $\overline{v_\theta^4} = \overline{v_\phi^4}$ and $\overline{v_r^2 v_\theta^2} = \overline{v_r^2 v_\phi^2}$ are related by two higher-order Jeans equations (Merrifield & Kent 1990).

In order to solve these equations we need additional information about the distribution function. We will restrict ourselves here to functions which can be constructed from the energy-dependent distribution function by multiplying it by a function of angular momentum $f(E, L) = f_0(E)L^{-2\beta}$ with $\beta = \text{const}$. The solution of the Jeans equation for the fourth-order moment (see Łokas 2002)

$$\frac{\mathrm{d}}{\mathrm{d}r}\left(\nu\overline{v_r^4}\right) + \frac{2\beta}{r}\nu\overline{v_r^4} + 3\nu\sigma_r^2\frac{\mathrm{d}\Phi}{\mathrm{d}r} = 0, \tag{18}$$

is

$$\nu\overline{v_r^4}(\beta = \text{const}) = 3r^{-2\beta}\int_r^\infty r^{2\beta}\nu\sigma_r^2(r)\frac{\mathrm{d}\Phi}{\mathrm{d}r}\,\mathrm{d}r. \tag{19}$$

By projection, we obtain the line-of-sight fourth moment

$$\overline{v_{\rm los}^4}(R) = \frac{2}{I(R)}\int_R^\infty\frac{\nu\overline{v_r^4}r}{\sqrt{r^2-R^2}}g(r, R, \beta)\,\mathrm{d}r, \tag{20}$$

where

$$g(r, R, \beta) = 1 - 2\beta\frac{R^2}{r^2} + \frac{\beta(1+\beta)}{2}\frac{R^4}{r^4}. \tag{21}$$

Introducing equations (15) and (19) into (20) and inverting the order of integration, we obtain

$$\overline{v_{\rm los}^4}(R) = \frac{6G^2}{I(R)}\int_R^\infty\frac{r^{-2\beta+1}}{\sqrt{r^2-R^2}}g(r, R, \beta)\,\mathrm{d}r \times\int_r^\infty\frac{\nu(q)M(q)}{q^{2-2\beta}}\,\mathrm{d}q\int_r^q\frac{M(p)}{p^2}\,\mathrm{d}p \tag{22}$$

and the calculation of $\overline{v_{\rm los}^4}(R)$ can be reduced to a (rather long) double integral. A useful way to express the fourth projected moment is to scale it with $\sigma_{\rm los}^4$ in order to obtain the projected kurtosis

$$\kappa_{\rm los}(R) = \frac{\overline{v_{\rm los}^4}(R)}{\sigma_{\rm los}^4(R)}, \tag{23}$$

whose value is 3 for a Gaussian distribution.

5 RESULTS

We use our sample of galaxy velocities to calculate the velocity moments of the E-S0 galaxies. The 355 available E-S0 galaxies were divided into bins of 39 objects. Fig. 3 shows the line-of-sight velocity dispersion (upper panel) and kurtosis (lower panel) together with their sampling errors calculated using estimators based on Monte Carlo simulations (see Appendix A). We find the sampling distribution of $\sigma_{\rm los}$ to be close to normal. In the case of kurtosis, shown in the lower panel of Fig. 3 the values are actually calculated and their errors propagated from the quantity $(\log\kappa_{\rm los})^{1/10}$ which we find to be normally distributed (see Appendix A). Normal sampling distributions of the estimators of both moments and very weak correlations between them justify the use of standard fitting procedures of these quantities based on χ^2 minimization.

Our purpose here is to reproduce the observed velocity moments using models described by equations (16) and (22), with the mass distribution given by the sum of the three contributions (2), (5) and (12) discussed in Section 3:

$$M(r) = M_{\rm G} + M_{\rm g} + M_{\rm D}. \tag{24}$$

The density profile $\nu(r)$ of the tracer population of early-type galaxies is given by equation (1) and the surface brightness $I(R)$ by its projection. While studying velocity dispersion is useful to constrain the mass, the kurtosis is mostly sensitive to the velocity anisotropy.

To give a feeling of its behaviour, we show in Fig. 3 the predictions of equation (22) (and the corresponding ones of equation 16) for the three cases of radial ($\beta = 1$), isotropic ($\beta = 0$) and circular ($\beta = -\infty$) orbits assuming dark matter distribution given by an NFW profile (equation 6 with $\alpha = 1$) for the virial mass $M_{\rm v} = 10^{15}\,{\rm M}_\odot$ and with concentration $c = 6$ (as suggested by formula 8 for the

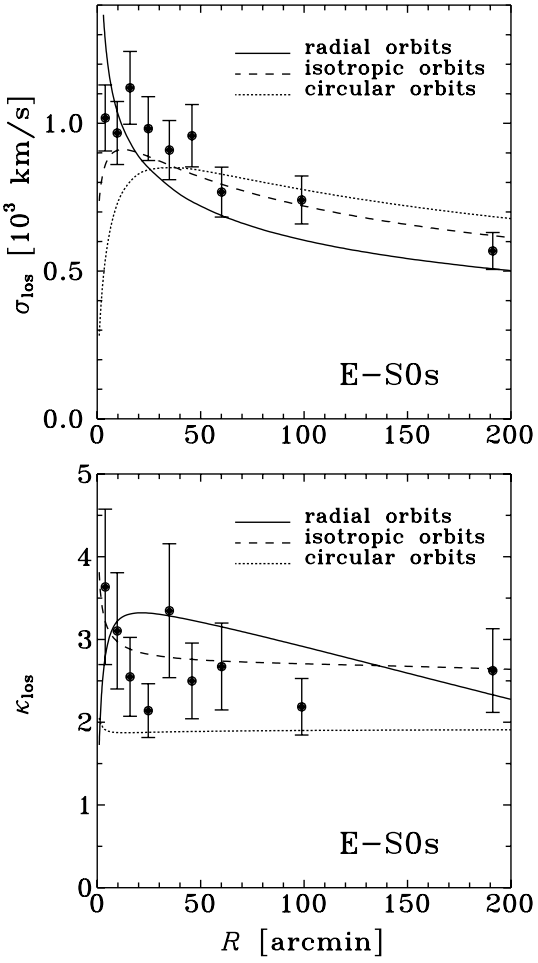

Figure 3. The line-of-sight velocity dispersion (upper panel) and the dimensionless line-of-sight kurtosis parameter (lower panel) of E-S0 galaxies. The curves represent models with stars, hot gas and dark matter with NFW distribution of mass $M_v = 10^{15}$ M$_\odot$ and concentration $c = 6$.

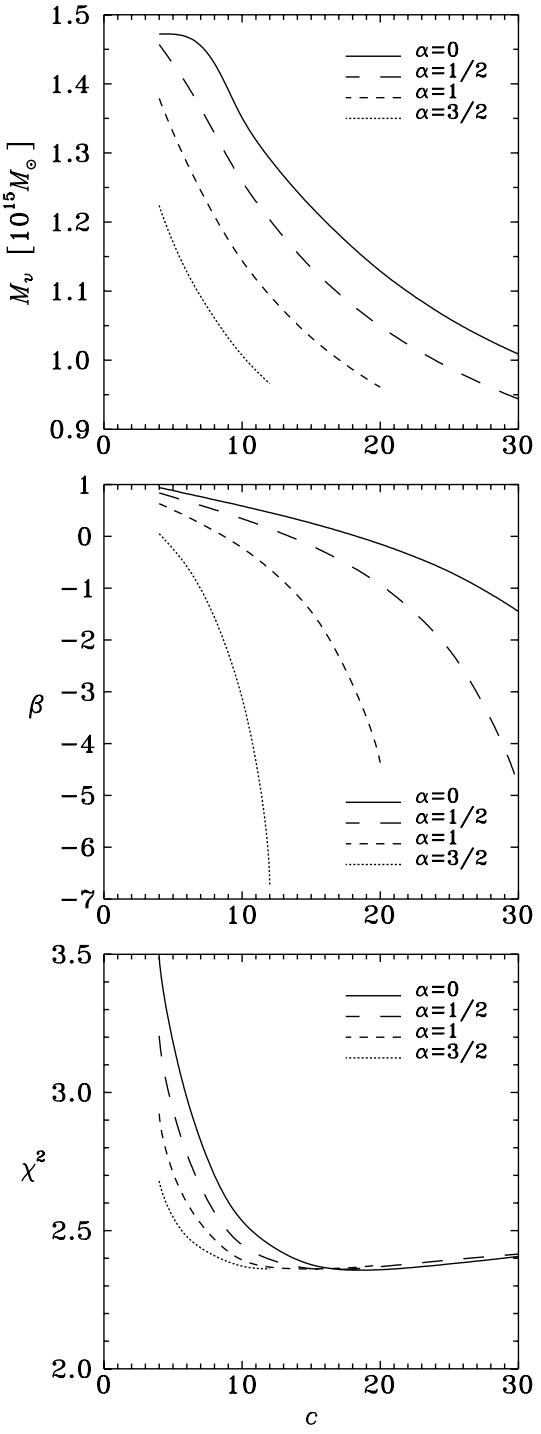

Figure 4. Results of fitting line-of-sight velocity dispersion data. The best-fitting parameters M_v and β are shown in the two upper panels as a function of concentration for different α. The lower panel gives the goodness of fit χ^2.

mass of this order). We see that for radial orbits the kurtosis profile is convex as opposed to the concave shapes in the case of isotropic and circular orbits. Because our data seem to prefer a concave shape, we can expect isotropic or tangential orbits to fit the data best.

We begin by fitting the line-of-sight velocity dispersion profile shown in the upper panel of Fig. 3. We consider different values of $\alpha = 0, 1/2, 1, 3/2$, and, for each of them, we determine the best-fitting anisotropy parameter β and dark virial mass M_v as a function of concentration c. The best-fitting values of M_v obtained are of the order of 10^{15} M$_\odot$, which corresponds to dark halo virial radius $r_v = 88$ arcmin or 2.6 Mpc. The virialized region is supposed to lie within this radius, so in the following analysis we discard the two outer radial bins.

Fig. 4 shows the results of fitting just the inner seven data points in the upper panel of Fig. 3 for $\alpha = 0, 1/2, 1$ and $3/2$. The best-fitting dark virial mass M_v (upper panel) and the velocity anisotropy parameter for early-type galaxies β (middle panel) are shown as a function of concentration. The lower panel of Fig. 4 shows the goodness of fit χ^2 (we do not use χ^2/N, with N the number of degrees of freedom, because it is not obvious how many parameters can be estimated with this procedure). As can be seen in Fig. 4, the biggest M_v obtained is 1.5×10^{15} M$_\odot$ which gives $r_v = 100$ arcmin or 2.9 Mpc. The data points are now all within this region and therefore there is no need for further adjustments in the number of data points analysed. The lowest panel of Fig. 4 proves that neither c nor α can be constrained from the analysis of velocity dispersion alone; χ^2 flattens for large c and reaches similar values for all α for a wide range of c.

As discussed in Appendix A, the sampling distributions of σ_{los} and $(\log \kappa_{los})^{1/10}$ are independent, hence we can use the same χ^2

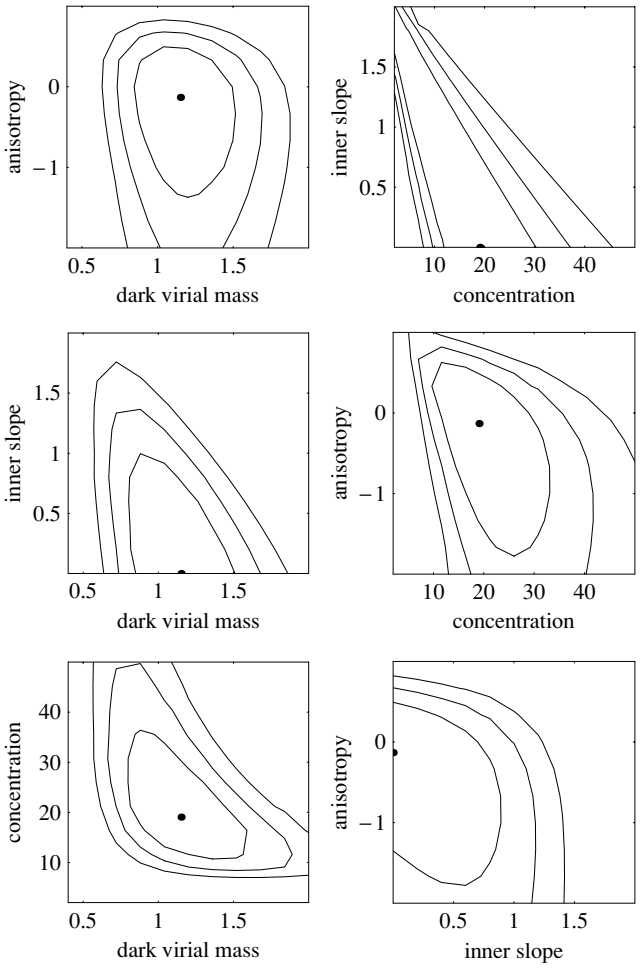

Figure 5. Cuts through the 1σ, 2σ and 3σ probability contours in the parameter space obtained from fitting $\sigma_{\rm los}$ and $(\log \kappa_{\rm los})^{1/10}$. Circles (and half-circles) indicate the best-fitting parameters. The mass is in units of 10^{15} M$_\odot$.

minimization scheme to find joint constraints following from fitting both quantities. Using the total of 14 data points at $R < 80$ arcmin, we jointly fit our four parameters, $M_{\rm v}$, β, α and c. Contrary to the case when only velocity dispersion was studied, the minimization procedure now converges. The minimum is found at $M_{\rm v} = 1.2 \times 10^{15}$ M$_\odot$ (corresponding to dark matter virial radius $r_{\rm v} = 92$ arcmin $=$ 2.7 Mpc), $\beta = -0.13$, $\alpha = 0$ and $c = 19$ with $\chi^2/N = 6.1/10$. For a better visualization of the constraints obtained for our four parameters, we plot in Fig. 5 the cuts through the four-dimensional confidence region in all six possible planes with probability contours corresponding to 1σ (68 per cent), 2σ (95 per cent) and 3σ (99.7 per cent), i.e. $\Delta\chi^2 = \chi^2 - \chi^2_{\rm min} = 4.72$, 9.70, 16.3, where $\chi^2_{\rm min} = 6.1$.

Although the cuts do not tell everything about the confidence region, Fig. 5 can be used to draw a number of interesting conclusions. The most striking is the behaviour of the confidence region in the c–α plane shown in the upper-right corner. Its shape shows that there is a strong degeneracy between the two parameters and indeed almost equally good fits can be obtained for the values of the inner slope other than $\alpha = 0$. The best-fitting values of the remaining parameters (together with the corresponding χ^2 value) when different α are assumed are listed in Table 1. The results confirm that indeed $\alpha = 0$ gives the best fit, but other inner slopes cannot be excluded.

Table 1. Best-fitting parameters from joint analysis of $\sigma_{\rm los}$ and $\kappa_{\rm los}$ of E-S0 galaxies. $M_{\rm v}$ is in units of 10^{15} M$_\odot$.

α	$M_{\rm v}$	β	c	χ^2
0	1.2	−0.13	19	6.1
1/2	1.2	−0.14	14	6.2
1	1.2	−0.16	9.4	6.4
3/2	1.2	−0.21	4.9	6.9

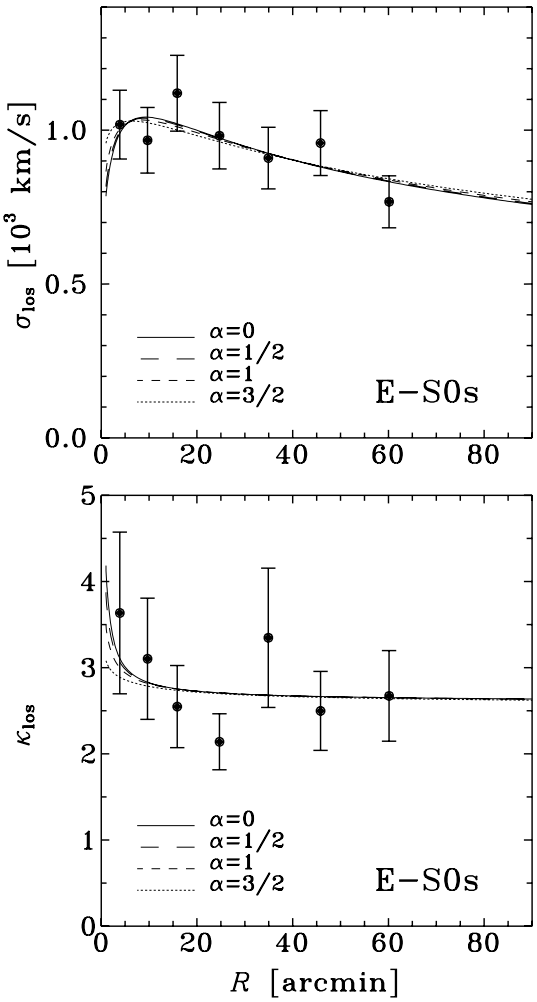

Figure 6. The best-fitting line-of-sight velocity dispersion (upper panel) and kurtosis (lower panel) profiles of E-S0 galaxies. The parameters of the models are listed in Table 1. The data are the same as in Fig. 3, except that only the seven inner data points are shown in each panel.

The steeper the inner slope (the higher the value of α), however, the lower is the concentration required to provide good fits to the moments.

The velocity moments obtained with the sets of parameters listed in Table 1 are shown in Fig. 6 together with the data; they overlap almost exactly. The dark matter profiles following from equation (6) with the parameters from Table 1 are plotted in the upper panel of Fig. 7. In the lower panel we also show the logarithmic slopes of the profiles. In both panels our best-fitting profiles are compared to the 'standard' NFW profile with concentration $c = 6$ (as suggested by formula 8 for the mass of the order of 10^{15} M$_\odot$). As can be seen

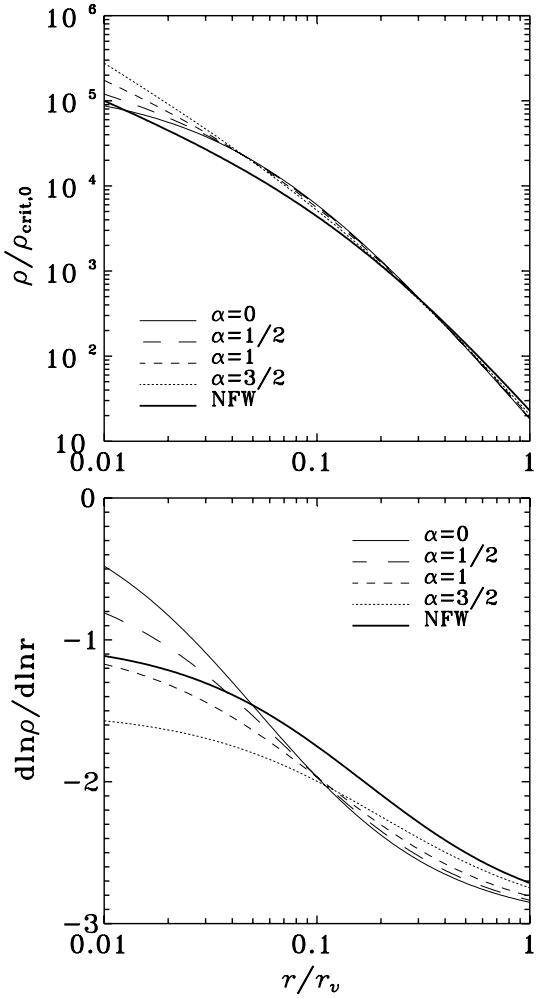

Figure 7. The best-fitting dark matter profiles with different inner slopes (upper panel) and their effective slopes (lower panel) as a function of radial distance (in units of the virial radius). The thick solid line in each panel shows the same quantities for the standard NFW profile with $c = 6$.

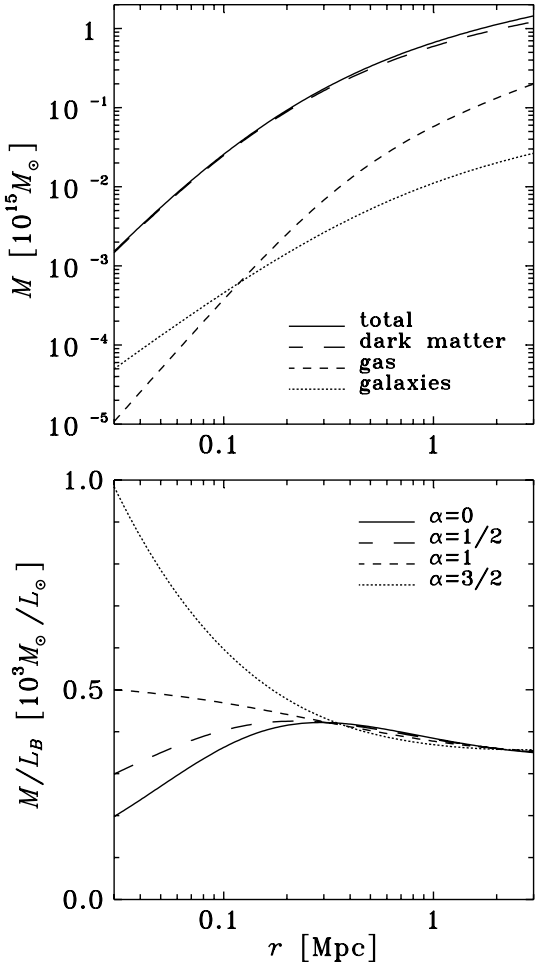

Figure 8. Upper panel: the mass distributions for the best-fitting model ($\alpha = 0$). Lower panel: the mass-to-light ratios for the best-fitting models with different α. The dark matter virial radii are $r_v = 2.7$ Mpc for all models shown.

in the upper panel, all our profiles overlap in a wide range of radial distances $0.03 r_v < r < r_v$, and are steeper beyond $0.05\ r_v$ (see the lower panel) than the standard NFW model deduced from cosmological N-body simulations. Indeed, our best-fitting NFW profile has concentration $c = 9.4$, higher by 50 per cent than the standard NFW profile for which $c = 6$ according to equation (8).

The remaining parameters M_v and β are better constrained. The three panels on the left in Fig. 5 show the probability contours for M_v in the planes with the other three parameters. We find the best estimate for the dark mass to be $M_v = (1.2 \pm 0.4) \times 10^{15}\ M_\odot$ (1σ error bars). The anisotropy parameter β is very close to isotropic, the best-fitting value $\beta = -0.13$ gives $\sigma_\theta = 1.06\,\sigma_r$, i.e. the best-fitting orbits of early-type galaxies are very weakly tangential, although fully consistent with isotropy, while radial orbits are excluded at the 2σ level.

The upper panel of Fig. 8 compares the mass distributions in stars, gas and dark matter with the total mass distribution for our best-fitting model with $\alpha = 0$. At the dark matter virial radius $r_v = 2.7$ Mpc, the total mass is $1.4 \times 10^{15}\ M_\odot$. The mass in galaxies is only 2 per cent of the total mass, the mass in gas is 13 per cent of the total (the galaxies thus represent less than one-seventh of the baryonic mass), and the dark matter contributes the remaining 85 per cent of the total mass. Therefore, the virial radius for the total mass is $0.85^{-1/3} = 1.06$ times that of the dark matter, i.e. 97 arcmin or 2.9 Mpc.

The cumulative mass-to-light ratio, i.e. the ratio of the total mass distribution to the luminosity distribution in galaxies, is

$$M/L_B = \frac{M(r)}{L_G(r)}, \tag{25}$$

where $M(r)$ is given by equation (24) with equations (2), (5) and (12), while $L_G(r) = M_G(r)/\Upsilon$. In the lower panel of Fig. 8 we show M/L_B for our best-fitting models for different α, with parameters from Table 1. The models differ towards the centre and only for $\alpha = 1$ does the distribution tend to a constant value in this limit, as we have used the NFW profile to fit the luminosity distribution of galaxies in Section 2. At radial distances larger than 0.3 Mpc, the cumulative mass-to-light ratio decreases slowly to reach $M/L_B \approx 351\ M_\odot/L_\odot$ at the total mass virial radius 2.9 Mpc.

6 DISCUSSION

We studied the velocity moments of early-type galaxies in the Coma cluster and used them to constrain the distribution of dark matter and velocity anisotropy. Our analysis differs from previous analyses

of optical data (e.g. The & White 1986; Merritt 1987; den Hartog & Katgert 1996; Carlberg et al. 1997; van der Marel et al. 2000; Biviano et al. 2003; Biviano & Girardi 2003), in that:

(i) we have, for a single cluster, a larger sample of galaxies, which, given their early morphological type, should be in dynamical equilibrium in the cluster potential;

(ii) we remove pairs from the computation of the velocity moments;

(iii) we include kurtosis in the analysis;

(iv) we model dark matter distribution using a generalized formula inspired by the results of cosmological *N*-body simulations;

(v) we include hot gas in our analysis.

In comparison to studies based upon stacking of many clusters, our analysis of the Coma cluster benefits from not having to introduce errors in any stacking procedure, and from a cleaner removal of interlopers. On the other hand, the analyses of stacked clusters have the advantage of averaging out particular inhomogeneities of individual clusters such as Coma, expected in hierarchical scenarios of structure formation. Indeed, the Coma cluster is known to have irregular structure both in projected space (Fitchett & Webster 1987; Mellier et al. 1988; Briel et al. 1992) and velocity space (Colless & Dunn 1996; Biviano et al. 1996). In particular, the cluster has two central dominant (cD) galaxies, NGC 4874 and 4889, of which the first one is the central galaxy of the main cluster and the second probably belonged to a subcluster which has recently merged with the main cluster (e.g. Colless & Dunn 1996). There are other subgroups, such as that associated with NGC 4839 at around 40 arcmin from NGC 4874, close enough to the cluster centre to contribute to our analysis.

The question whether the E-S0 sample is relaxed and how the existing substructure may affect our results can only be fully addressed by cosmological *N*-body simulations including galaxy formation, where all 3D information would be available. Although such an analysis has not yet been performed, the effect of the incomplete virialization of structures of dark matter particles seen in cosmological simulations on the estimates of the mass of a single cluster through the Jeans equation has been addressed by Tormen, Bouchet & White (1997). They have shown (see the bottom row of their figure 17) that, even for significantly perturbed haloes, the mass $M(r)$ at distances larger than 2 per cent of the virial radius inferred by the proper Jeans analysis is within 30 per cent (rms) of the true mass and departs from it by less than 20 per cent (rms) for average or relaxed haloes. As the dark matter distribution is known to possess more substructure than is observed in the galaxy distribution (cosmological simulations predict many more Milky Way satellites than are observed; see, for example, Moore et al. 1999) and because structures cease to grow sooner in flat universes with a cosmological constant, in comparison with analogous structures growing within the Einstein–de Sitter model (assumed in the simulations by Tormen et al.), they are more regular today (see Thomas et al. 1998) than shown in the first three columns of the bottom row of figure 17 in Tormen et al. We therefore believe that the discrepancy between our derived mass and the true cluster mass due to substructure and departures from equilibrium is significantly smaller than the uncertainty due to sampling errors of the velocity moments.

Our results for the dark and total mass of the cluster are consistent with previous estimates. Using a combination of X-ray and optical data, Hughes (1989) found for his preferred model a total mass within $3.6h_{70}^{-1}$ Mpc (where we used the notation $H_0 = 70h_{70}$ km s^{-1} Mpc^{-1}) to be $(1.3 \pm 0.2) \times 10^{15}h_{70}^{-1}$ M$_\odot$, but a much wider range of masses if more general mass distributions were allowed. Using *ROSAT* observations of Coma and assuming hydrostatic equilibrium of the gas, Briel et al. (1992) derived a mass within the same radial distance to be $(1.3 \pm 0.4) \times 10^{15}h_{70}^{-1}$ M$_\odot$. Also, by analysing the infall patterns around Coma, Geller, Diaferio & Kurtz (1999) find a mass of $(1.7 \pm 0.4) \times 10^{15}h_{70}^{-1}$ M$_\odot$ within the same distance to the cluster centre as above. Extrapolating our results to this radial distance, we find an enclosed mass of $(1.6 \pm 0.5) \times 10^{15}h_{70}^{-1}$ M$_\odot$, in good agreement with these three earlier estimates.

We find a strong degeneracy between the inner slope and the concentration of the dark matter profile, with many combinations of the two reproducing our velocity profiles almost equally well. In the range of inner slopes $0 \leqslant \alpha \leqslant 3/2$ we find that the best-fitting models have the two parameters related almost linearly as $c = 19 - 9.6\alpha$ with very little variation in the remaining fitting parameters, $M_{\rm v}$ and β. The particular shape of the degeneracy between c and α is due to the specific properties of the family of dark matter profiles used in this analysis, coupled with our lack of velocity data at radii smaller than the scale radius ($r_{\rm s}$) of the dark matter. Using smaller radial bins would allow us to probe smaller radial distances, but at the expense of larger sampling errors in the velocity moments. As is clear from Fig. 7, the best-fitting dark matter profiles obtained for different inner slopes are almost the same for a wide range of distances (larger than 3 per cent of the virial radius) and this can only be achieved with the combination of the parameters as given in Table 1. Note that our best fit to the data for the flat dark matter density profile might mean that the data may be even better fitted with the unphysical model where the dark matter density profile rises with radius in the cluster centre, i.e. $\alpha < 0$ in equation (6).

Our best-fitting NFW profile ($\alpha = 1$) has a concentration $c = 9.4$ (in agreement with the above formula), 50 per cent higher than $c = 6$ found in *N*-body simulations. It should be kept in mind, however, that the concentration parameters in the simulations are subject to substantial scatter and that the formula (8) (giving $c = 6$) at masses of the order of 10^{15} M$_\odot$ is actually an extrapolation of results obtained for lower mass haloes (see Bullock et al. 2001). However, the 'standard' NFW model with $c = 6$ is still within our 1σ confidence region in Fig. 5.

In comparison, fits of the NFW profile to X-ray data of clusters, assumed isothermal, by Ettori & Fabian (1999), rescaled by Wu & Xue (2000), as well as by Sato et al. (2000), both yield $c \simeq 4$ for the mass that we find for Coma within the virial radius (the latter after correction from $\Delta_{\rm c} = 200$ to $\Delta_{\rm c} = 102$), which is only within our 2σ confidence region. It may be that the assumption of isothermal hot gas causes a lower concentration parameter.

In an analysis similar in spirit to ours, Biviano et al. (2003) report $c = 4 \pm 2$ for their stacked ensemble of 59 ENACS clusters, fitted to a NFW model for the total mass density. Similarly, Biviano & Girardi (2003) show that NFW models with $c = 5.5$ are consistent with a stacked ensemble of 43 2dF Galaxy Redshift Survey (2dFGRS) clusters. Moreover, the ENACS and 2dFGRS clusters analysed in both studies are on average less massive (i.e. with lower velocity dispersions) than Coma, and given that cosmological simulations find a decreasing c for increasing mass, the discrepancy with our result is even stronger.

The difference of these four studies with our result may be explained by the fact that the authors mentioned above fit the *total* mass density profile to the NFW form, whereas our fit was performed for the distribution of the dark component only. If the gas is distributed similarly in the X-ray, ENACS and 2dFGRS clusters as in Coma, i.e. it has a flat inner core, and the gas on average contributes a substantial part of the total mass, fitting the total mass distribution may result in flatter profiles than the dark haloes really have. The

discrepancy may be also caused by the exclusion of cD galaxies by Biviano et al. (2003), although we feel that removing one or two galaxies from our central bin of 39 galaxies will not affect our results. Alternatively, their mass model (obtained with the assumption of isotropic orbits) may not be coherent with the kurtosis profile of their stacked cluster.

Our best-fitting models have orbits that are very close to isotropic, as is expected, in the central regions, where the two-body relaxation time for the galaxy system is considerably smaller than the age of the Universe, and also because cosmological simulations indicate that dark matter particles typically have isotropic orbits in the centres of clusters (Thomas et al. 1998; Huss, Jain & Steinmetz 1999). In other words, we find no significant anisotropy bias for the galaxies relative to the expectations of isotropy for the dark matter. Note that, if we force isotropic orbits for the galaxies, we then obtain similar constraints for the inner slope, concentration parameter and mass of the dark matter component within the virial radius as those shown in Fig. 5.

We might wish to better reproduce the kurtosis profile. It is clear from Fig. 6 that, while the velocity dispersion profile is well reproduced, there is room for improvement for the kurtosis profile. However, as discussed in Section 4, the kurtosis is mainly sensitive to the velocity anisotropy, which was modelled here by a single constant parameter. Besides, the curves shown in Fig. 6 are the results of joint fitting of both moments and do not aim at reproducing the kurtosis alone. In spite of this, the inclusion of the kurtosis in our analysis allowed us to constrain the velocity anisotropy and other parameters of the model.

From our best estimate of the mass distribution, the baryons (galaxies and gas) contribute 15 per cent of the total mass at the dark matter virial radius $r_{\rm v} = 2.7$ Mpc (see Fig. 8). If we assume that the cluster content is representative of the Universe as a whole, we can use this baryon fraction to estimate the density parameter Ω_0 (see, for example, White et al. 1993). Taking the baryonic density parameter at its currently best value from nucleosynthesis $\Omega_{\rm b} = 0.04$ (with $h = 0.7$) we obtain $\Omega_0 = 0.26 \pm 0.09$ where the error comes from our 30 per cent uncertainty in the dark virial mass value, 20 per cent uncertainty in the gas mass (as estimated by White et al. 1993) and 10 per cent error in the $\Omega_{\rm b}$ value (Burles, Nollett & Turner 2001).

Similarly, we may assume that clusters are good tracers, within their virial radius, of the ratio of mass to blue luminosity. Given that the closure mass-to-light ratio (critical density over luminosity density) in the blue band is roughly 1100 h_{70} to 10 per cent accuracy, consistent with the recent estimates of luminosity density from the 2dFGRS (Norberg et al. 2002) and Sloan Digital Sky Survey (Blanton et al. 2001) (after correction to the blue band), our mass-to-light ratio within the virial radius of $351h_{70}$ with 30 per cent accuracy yields $\Omega_0 = 0.32 \pm 0.1$.

Combining these two estimates of the density parameter, we arrive at $\Omega_0 = 0.29 \pm 0.1$ in excellent agreement with other determinations, for example the recent value obtained from the Wilkinson Microwave Anisotropy Probe (WMAP) cosmic microwave background experiment (Spergel et al. 2003).

ACKNOWLEDGMENTS

We wish to thank Y. Hoffman and the anonymous referee for useful comments and suggestions. We acknowledge hospitality of the Institut d'Astrophysique de Paris where ELŁ benefited from the Jumelage exchange programme as well as the NATO Advanced Fellowship and where most of this work was done. Partial support was obtained from the Polish State Committee for Scientific Research within grant No 2P03D02319. This research has made use of the NED which is operated by the Jet Propulsion Laboratory, California Institute of Technology, under contract with the National Aeronautics and Space Administration. We have also used the LEDA data base (http://leda.univ-lyon1.fr) and SIMBAD operated at CDS, Strasbourg, France, as well as NASA's Astrophysics Data System Service (ADS).

REFERENCES

Arnaud M. et al., 2001, A&A, 365, L67
Bartelmann M., 1996, A&A, 313, 697
Binney J., Mamon G. A., 1982, MNRAS, 200, 361
Biviano A., 1998, in Mazure, A., et al., eds, Proc. Marseilles Meeting, A New Vision of an Old Cluster: Untangling Coma Berenices. World Scientific, Singapore, p. 1
Biviano A., Girardi M., 2003, ApJ, 585, 205
Biviano A., Durret F., Gerbal D., Le Fèvre O., Lobo C., Mazure A., Slezak E., 1996, A&A, 311, 95
Biviano A., Katgert P., Thomas T., Mazure A., 2003, in Avila-Reese V. et al., eds, Proc. Cozumel Conf., Galaxy Evolution: Theory and Observations. RevMexAA, in press (astro-ph/0301343)
Blanton M. et al., 2001, AJ, 121, 2358
Briel U. G., Henry J. P., Böhringer H., 1992, A&A, 259, L31
Broadhurst T., Huang X., Frye B., Ellis R., 2000, ApJ, 534, L15
Bullock J. S., Kolatt T. S., Sigad Y., Somerville R. S., Kravtsov A. V., Klypin A. A., Primack J. R., Dekel A., 2001, MNRAS, 321, 559
Burkert A., 1995, ApJ, 447, L25
Burles S., Nollett K. M., Turner M. S., 2001, ApJ, 552, L1
Carlberg R. G. et al., 1997, ApJ, 485, L13
Colless M., Dunn A. M., 1996, ApJ, 458, 435
den Hartog R., Katgert P., 1996, MNRAS, 279, 349
Eke V. R., Cole S., Frenk C. S., 1996, MNRAS, 282, 263
Ettori S., Fabian A. C., 1999, MNRAS, 305, 834
Fitchett M., Webster R., 1987, ApJ, 317, 653
Fukushige T., Makino J., 1997, ApJ, 477, L9
Geller M. J., Diaferio A., Kurtz M. J., 1999, ApJ, 517, L23
Henry J. P., Henriksen M. J., 1986, ApJ, 301, 689
Huchra J. P., 1985, in Richter O. G., Binggeli B., eds, Proc. ESO Workshop on the Virgo Cluster of Galaxies. ESO, Munich, p. 181
Hughes J. P., 1989, ApJ, 337, 21
Huss A., Jain B., Steinmetz M., 1999, MNRAS, 308, 1011
Jimenez R., Verde L., Oh S. P., 2003, MNRAS, 339, 243
Jing Y. P., Suto Y., 2000, ApJ, 529, L69
Kent S. M., Gunn J. E., 1982, 87, 945
Łokas E. L., 2002, MNRAS, 333, 697
Łokas E. L., Hoffman Y., 2001, in Spooner N. J. C., Kudryavtsev V., eds, Proc. 3rd International Workshop, The Identification of Dark Matter. World Scientific, Singapore, p. 121
Łokas E. L., Mamon G. A., 2001, MNRAS, 321, 155
Magorrian J., Ballantyne D., 2001, MNRAS, 322, 702
McGaugh S. S., de Blok W. J. G., 1998, ApJ, 499, 41
McLaughlin D. E., 1999, ApJ, 512, L9
Mellier Y., Mathez G., Mazure A., Chauvineau B., Proust D., 1988, A&A, 199, 67
Merrifield M. R., Kent S. M., 1990, AJ, 99, 1548
Merritt D., 1987, ApJ, 313, 121
Moore B., Governato F., Quinn T., Stadel J., Lake G., 1998, ApJ, 499, L5
Moore B., Ghigna S., Governato F., Lake G., Quinn T., Stadel J., Tozzi P., 1999, ApJ, 524, L19
Navarro J. F., Frenk C. S., White S. D. M., 1997, ApJ, 490, 493
Norberg P. et al., 2002, MNRAS, 336, 907
Sato S., Akimoto F., Furuzawa A., Tawara Y., Watanabe M., Kumai Y., 2000, ApJ, 537, L73
Spergel D. N. et al., 2003, ApJ, submitted (astro-ph/0302209)
Struble M. F., Rood H. J., 1999, ApJS, 125, 35

Stuart A., Ord K., 1994, Kendall's Advanced Theory of Statistics, Vol. I: Distribution Theory. Oxford Univ. Press, New York, ch. 10
Tamura T., Makishima K., Fukazawa Y., Ikebe Y., Xu H., 2000, ApJ, 535, 602
The L. S., White S. D. M., 1986, AJ, 92, 1248
Thomas P. A. et al., 1998, MNRAS, 296, 1061
Tormen G., Bouchet F. R., White S. D. M., 1997, MNRAS, 286, 865
Tully R. B., Shaya E. J., 1984, ApJ, 281, 31
Tyson J. A., Kochanski G. P., dell'Antonio I. P., 1998, ApJ, 498, L107
van der Marel R. P., Magorrian J., Carlberg R. G., Yee H. K. C., Ellingson E., 2000, AJ, 119, 2038
White S. D. M., Navarro J. F., Evrard A. E., Frenk C. S., 1993, Nat, 366, 429
Williams L. L. R., Navarro J. F., Bartelmann M., 1999, ApJ, 527, 535
Wu X.-P., Xue Y.-J., 2000, ApJ, 529, L5

APPENDIX A: THE SAMPLING DISTRIBUTIONS

The validity of modelling presented in this paper rests on proper estimation of the velocity moments and their errors from observations. If their sampling distributions tend to normality, the statistics obtained from a sample (e.g. moments) can be characterized by an expectation value and a 'standard' error (Stuart & Ord 1994). For simplest statistics, such as the second central moment, these can be calculated exactly from the population moments assuming the population properties. As we are interested here also in quantities whose standard errors are not easily calculated analytically, we resort to Monte Carlo methods.

The most natural estimators of the variance and kurtosis from a sample of n line-of-sight velocity measurements v_i are

$$S^2 = \frac{1}{n}\sum_{i=1}^{n}(v_i - \overline{v})^2 \tag{A1}$$

and

$$K = \frac{\frac{1}{n}\sum_{i=1}^{n}(v_i - \overline{v})^4}{(S^2)^2} \tag{A2}$$

where

$$\overline{v} = \frac{1}{n}\sum_{i=1}^{n} v_i \tag{A3}$$

is the mean of galaxy velocities in the sample.

To investigate the distribution of these estimators for our binning of galaxies, i.e. when $n = 39$, we ran Monte Carlo simulations by selecting $\mathcal{N} = 10^4$ times $n = 39$ numbers from a Gaussian distribution with zero mean and dispersion of unity. As velocity distributions of gravitationally bound objects in general do not dramatically depart from a Gaussian, this is a sufficient approximation for constructing unbiased estimators of moments.

For each of the $\mathcal{N}$ samples we compute the statistic $\theta_j^\star$, namely S^2 or K according to prescriptions given by equations (A1) and (A2). The Monte Carlo estimate of our statistic is then the mean of all values obtained

$$\theta^\star = \frac{1}{\mathcal{N}}\sum_{j=1}^{\mathcal{N}}\theta_j^\star \tag{A4}$$

and its variance is

$$\mathrm{var}(\theta^\star) = \frac{1}{\mathcal{N}-1}\sum_{j=1}^{\mathcal{N}}\left(\theta_j^\star - \theta^\star\right)^2. \tag{A5}$$

We find that the best estimates obtained in this way are biased, especially for kurtosis (it is interesting to note that the value of kurtosis is underestimated by a few per cent even for much larger samples with n of the order of a few hundred). In addition, while the sampling distribution of velocity dispersion is Gaussian to a very good approximation, that for kurtosis is strongly skewed. Using this knowledge we construct unbiased and Gaussian-distributed estimators of line-of-sight velocity dispersion s and kurtosis-like variable k

$$s = \left(\frac{n}{n-1}S^2\right)^{1/2} \tag{A6}$$

$$k = \left[\log\left(\frac{3}{2.75}K\right)\right]^{1/10}. \tag{A7}$$

The factor $n - 1$ in equation (A6) is the well-known correction for bias when estimating the sample variance, valid independently of the underlying distribution. In equation (A7) the factor $3/2.75$ corrects for the bias in the kurtosis estimate, i.e. unbiased estimate of kurtosis is $K' = 3K/2.75$, while the rather complicated function of K' assures that the sampling distribution of k is approximately Gaussian. Examples of sampling distributions of s and k from our Monte Carlo simulation are shown in Fig. A1. We find that the standard errors in the case of s are of the order of 11 per cent (in agreement with an analytical result derivable with the assumption of Gaussian velocity distribution) while in the case of k they are approximately 2 per cent.

The measured values of $\sigma_{\rm los}$ and $\kappa_{\rm los}$ calculated from our velocity data using equations (A6)–(A7) and (A1)–(A2) are shown in Fig. 3. The 1σ error bars for the velocity dispersion are $0.11s$. The values of kurtosis are $K' = 3K/2.75$ with approximate 1σ error bars propagated from the 2 per cent error in k.

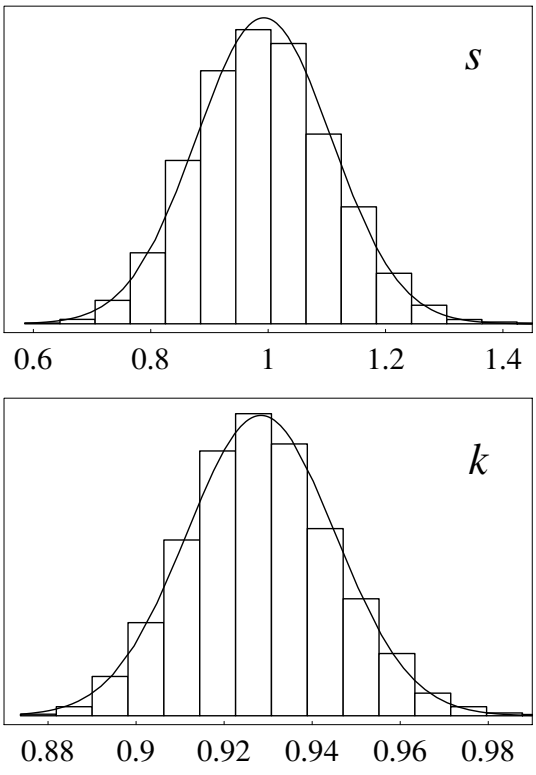

Figure A1. Example of sampling distributions of s and k obtained from a Monte Carlo simulation of sampling from a Gaussian parent distribution with $n = 39$ and $N = 10^4$.

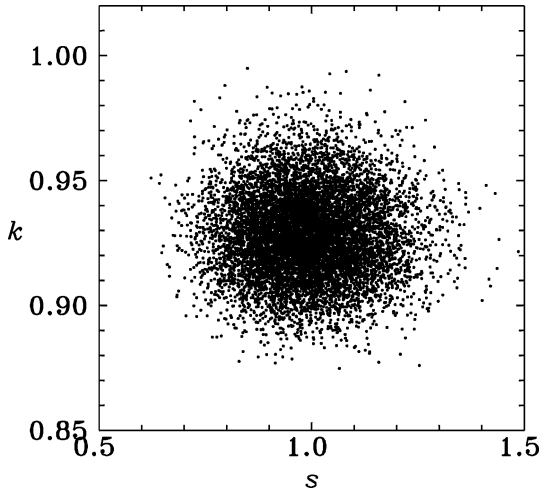

Figure A2. The joint distribution of s and k obtained from a Monte Carlo simulation of sampling from a Gaussian parent distribution with $n = 39$ and $N = 10^4$.

It is also important to check whether the sampling distributions of the two statistics are independent. In general, the covariance between, for example, even moments derived from the same sample does not vanish, even for Gaussian distributions (Stuart & Ord 1994). However, the lowest-order term is expected to decrease with the size of the sample n. To check whether $n = 39$ in our case is indeed large enough to assure independence of s and k, we construct the joint sampling distribution of the two statistics. Fig. A2 presents the joint distribution in the form of $\mathcal{N}$ points with coordinates given by (s, k) pairs calculated from each sample. As indicated by the figure the variables are very weakly correlated, and we find the correlation coefficient of $|\varrho| \leqslant 0.02$.

To check the behaviour of s and k for velocity distributions departing from Gaussianity, we repeated the Monte Carlo simulation, again sampling $n = 39$ numbers from a Gaussian distribution, but modifying each sample by removing the six most inner points and adding three uniformly distributed in the range $(1\sigma, 2\sigma)$ and three in the range $(-2\sigma, -1\sigma)$. Such distributions have unbiased kurtosis estimates of the order of $K' = 2.2$, close to the lowest value obtained from our data (and most strongly departing from the Gaussian value of 3). We find that estimators s and k are again Gaussian-distributed to a very good approximation and very weakly correlated with $|\varrho| \leqslant 0.07$. The sampling distributions of s and k as well as the joint distribution look very similar to the purely Gaussian case. The correlation coefficient can increase significantly only in the presence of additional outliers (more numerous than predicted by the Gaussian distribution) in the range $(2\sigma, 3\sigma)$ and $(-3\sigma, -2\sigma)$. We have checked that the number of galaxies with velocities in this range is 1 or 2 in each bin, in excellent agreement with the Gaussian prediction.

We can therefore assume that, to a good approximation, all our data points measuring velocity dispersion and kurtosis are independent, which justifies the use of standard χ^2 minimization to fit the models to the data.

This paper has been typeset from a TEX/LATEX file prepared by the author.